From topological phase to transverse Anderson localization in a two-dimensional quasiperiodic system

Shujie Cheng,[1] Reza Asgari,[2,1] and Gao Xianlong[1,*]
[1]*Department of Physics, Zhejiang Normal University, Jinhua 321004, China*
[2]*School of Physics, Institute for Research in Fundamental Sciences (IPM), Tehran 19395-5531, Iran*

(Received 21 December 2022; revised 8 July 2023; accepted 17 July 2023; published 27 July 2023)

In this paper, we provide theoretical approaches to identify the influence of the quasidisorder on a two-dimensional system. We discover that in the system there is a topological phase transition accompanied by a transverse Anderson localization. The topological features are characterized by the band gap, the edge-state spectra, the transport conductance, and the Chern number. The localization transition is clearly demonstrated by the investigations of the partial inverse participation ratio, the average of level spacing ratio, and the fraction dimension. The results reveal the topological nature of the bulk delocalized states. Our work facilitates the understanding of the synchronicity between the topological phase transition and the transverse Anderson localization in two-dimensional disordered systems.

DOI: 10.1103/PhysRevB.108.024204

I. INTRODUCTION

Band insulators have received a lot of attention due to their peculiar topological characteristics. Two representative insulators are the Chern class [1–3] and the quantum spin-Hall class [4–6]. The topological properties are reflected in that although these band insulators present the characteristics of an insulator in the bulk, there are still robust conducting states, distributed at the edges of the band insulators. The valence and conduction bands are connected by the Fermi levels of these edge modes, giving the insulators metallic properties [7]. Furthermore, the Chern number (C) can be used to predict whether the edge modes would exist or not. A nonzero C shows the presence of the edge modes, whereas $C = 0$ denotes their absence, according to the work of Thouless–Kohmoto–Nightingale–den Nijs (TKNN) [8].

The metallic characteristics indicated above are found to be robust against the disorder, implying that the topological properties of the system are still preserved as long as the bulk gap keeps open within a certain disorder strength [9]. The bulk gap will eventually close as the disorder strength increases, putting the system into a topologically trivial phase [10,11]. There has recently been an increase in interest in research on localization in 2D systems with Anderson disorder [12–24]. In a quantum spin-Hall system with broken time-reversal symmetry [25], specifically, the coexistence of nontrivial topology and Anderson localization was discovered, and the extended states were protected by the nontrivial topology [20]. Recently, there is interest in studying the influence of the quasidisorder on the 2D topological insulators. A quasidisorder is an additional type of disorder that belongs to the category of correlated disorders [26]. It was found that quasidisorder will make the system be fully localized [27–33] and be a critical metal [27], and even be a topological Anderson insulator [27–29], thus triggering the topological phase transition accordingly. In this paper, we are interested in the transverse Anderson localization triggered by the quasidisorder, which has recently been studied in a 2D quasidisordered topological superconductor with magnetic fields [28]. We note that in this 2D topological superconductor, the quasidisorder triggered transverse Anderson localization is not synchronous with the topological phase transition [28]. Based on these findings, we are motivated to study, in a quasidisordered 2D topological system without superconducting mechanisms and magnetic fields, whether there is a quasidisorder-triggered transverse Anderson localization which is followed by a topological phase transition. After all, Ref. [15] noted that 2D disordered systems may contain multifractal wave functions.

The rest of the paper is organized as follows. We present the model and its Hamiltonian in Sec. II. To analyze the topological properties of the model, we study the zigzag-edge spectra, transport conductance, and the Chern number in Sec. III. To analyze the transverse Anderson localization transition, we study the partial inverse participation ratio, the average of level spacing ratio, and the fraction dimension in Sec. IV. A summary is presented in Sec. V.

II. MODEL

The schematic diagram of the two-dimensional (2D) quasidisordered Chern insulator system is shown in Fig. 1. The primitive lattice vectors, $\boldsymbol{e_1}$ and $\boldsymbol{e_2}$, constitute the unit cell where there are three types of independent sublattices [34–37], marked by R, B, and G, respectively. a is the spacing between two nearest-neighbor sites ($a = 1$ in general). The total Hamiltonian $\hat{H} = \hat{H}_1 + \hat{H}_2$ of the system at zero temperature consists of two parts: One is the hopping terms given by

$$\hat{H}_1 = \sum_{j,j'} \big(J\hat{c}^{\dagger}_{\mathrm{R_j}}\hat{c}_{\mathrm{B}_{j'}} + J_1\hat{c}^{\dagger}_{\mathrm{G_j}}\hat{c}_{\mathrm{R}_{j'}} + J_1\hat{c}^{\dagger}_{\mathrm{G_j}}\hat{c}_{\mathrm{B}_{j'}} + J_2 e^{i\varphi}\hat{c}^{\dagger}_{\mathrm{R_j}}\hat{c}_{\mathrm{R}_{j'}} + J_2 e^{i\varphi}\hat{c}^{\dagger}_{\mathrm{B_j}}\hat{c}_{\mathrm{B}_{j'}} + \mathrm{H.c.}\big), \quad (1)$$

*Corresponding author: gaoxl@zjnu.edu.cn

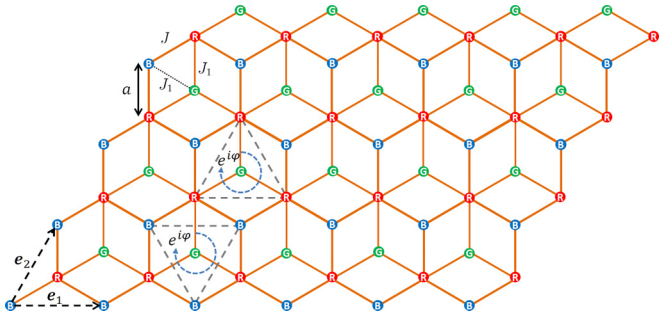

FIG. 1. Sketch of the model lattice system. The primitive lattice vectors $\boldsymbol{e_1}$ and $\boldsymbol{e_2}$ form a unit cell, which contains three types of independent sublattices, marked by R, B, and G, respectively. The hopping strength between nearest-neighbor R and B sites is J, and the one between nearest-neighbor G and R (or B) sites is J_1. The hopping strength between two nearest-neighbor R (or B) sites is $J_2 e^{i\varphi}$.

and the other is the quasidisordered (quasiperiodic) potentials defined by

$$\hat{H}_2 = \sum_{\mathcal{S}_{m,n}} V \cos(2\pi\alpha n)\hat{c}^{\dagger}_{\mathcal{S}_{m,n}}\hat{c}_{\mathcal{S}_{m,n}}, \tag{2}$$

where J is the unit of energy, $\mathcal{S}_{m,n} = m\boldsymbol{e_1} + n\boldsymbol{e_2}$ (m and n are integers) is the position of the $\mathcal{S}$ site ($\mathcal{S} \in \{\mathrm{R}, \mathrm{B}, \mathrm{G}\}$), V is the strength of the quasiperiodic potential, and $\alpha = (\sqrt{5}-1)/2$. This system has multiple parameters and we want to look at the quantum criticality cased by the quasiperiodic potential, the topological qualities, and the localization phase transition. Without losing generality, we take $J_1 = 0.3$, $J_2 = 0.275$, and $\varphi = \pi/2$ in the following.

III. TOPOLOGICAL PROPERTIES

We plot the energy gap of the lower two minibands as a function of V in Fig. 2(a) by considering a system with the size $N_{\boldsymbol{e_1}} \times N_{\boldsymbol{e_2}} = 40 \times 144$, where $N_{\boldsymbol{e_1}}$ is the number of unit cells along $\boldsymbol{e_1}$ (the longitudinal direction) and $N_{\boldsymbol{e_2}}$ is the one along $\boldsymbol{e_2}$ (the transverse direction) and selecting periodic boundary conditions (PBCs) in two directions. Intuitively, we can see that the system divides into two distinct phases at a critical point V_c ($V_c \approx 0.82J$ in the numerical calculations). The gap is always open when the potential strength V is smaller than the critical point, but it closes when V crosses the critical point. We do the finite-size analysis on the energy gap to determine whether it is affected by the system's size. Figures 2(b) and 2(c) show our results of the energy gap for various V. In particular, to calculate the gaps in Fig. 2(b), we keep $N_{\boldsymbol{e_2}}$ unchanged. In order to determine the gaps in Fig. 2(c), we maintain the invariant of $N_{\boldsymbol{e_1}}$ and set $N_{\boldsymbol{e_2}}$ to the sth Fibonacci number F_s. Of course, the gaps almost remain constants as the size of the system increases. It implies that the energy gap is unaffected by the size of the system. We conclude from the energy gap that the topological properties of the initial uniform case ($V = 0$) are preserved in the gapped phase at $V > 0$. Its topological characteristics in the uniform situation are intermediately reflected from the Bloch Chern number. In other words, the topological characteristics of the system are described using the TKNN formula [8].

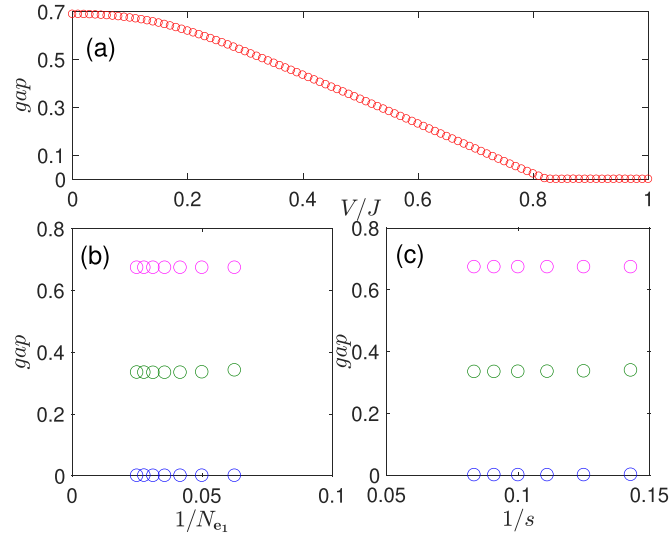

FIG. 2. (a) The energy gap of the lower two minibands as a function of V under PBC. The considered system has a size of 40×144 (40 unit cells along $\boldsymbol{e_1}$ and 144 unit cells along $\boldsymbol{e_2}$). Finite-size analysis about the energy gap with $V = 0.1J$ (magenta circles), $V = 0.5J$ (green circles), and $V = J$ (blue circles) in (b) and (c). To obtain (b), we keep $N_{\boldsymbol{e_2}}$ invariant and change $N_{\boldsymbol{e_1}}$. While calculating (c), we only change $N_{\boldsymbol{e_2}}$, and make $N_{\boldsymbol{e_2}}$ be equal to the sth Fibonacci number. The energy gaps almost remain constants as the size of the system increases.

Based on the energy gap, we infer that the gapped phase at $V > 0$ preserves the topological characteristics of the original uniform case ($V = 0$). We know that for the uniform case, its topological properties are intermediately reflected from the Bloch Chern number [8]. In this case, the Chern number of the lowest bands will be $C_1 = 1$.

We initially attempt to use the singly periodic spectrum to confirm the aforementioned inference. The lattice size is 64×89 and we leave it with PBCs in the longitudinal direction and with a zigzag edge in the transverse direction. As a result, the momentum $k_{\boldsymbol{e_1}}$ in the $\boldsymbol{e_1}$ direction is a good quantum number. The zigzag-edge spectrum in the $V = 0$ case is shown in Fig. 3(a). The red line depicts the 1/3-filling Fermi energy level in the bulk gap, which contains two edge modes with opposite momentum $k_{\boldsymbol{e_1}}$, and oppositely directional group velocities. One can observe two edges within the bulk gap at 1/3 filling for the quasiperiodic situations [see the cases with $V = 0.3J$ and $V = 0.5J$ in Figs. 3(b) and 3(c), respectively]. It means that there are preserved topological characteristics in the quasiperiodic case. However, in the quasiperiodic circumstances, as opposed to the uniform case, the corresponding momenta of the two edge modes are no longer symmetric about $k_{\boldsymbol{e_1}} = 0$. The zigzag-edge spectrum in the $V = J$ case has metallic characteristics but lacks a full bulk gap [see Fig. 3(d)], which is self-consistent with the energy gap under PBCs [see Fig. 2(a)].

The transport conductance [38–44] is an observable to characterize the topological features as expect for the edge modes. The Hamiltonian $\hat{H}$ is also used to define the (left and right) leads for convenience without losing generality. The conductance G_E of the system (central scattering region) can

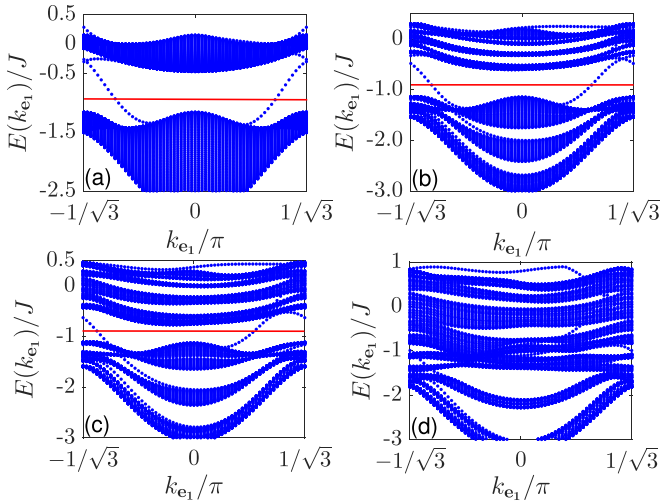

FIG. 3. Zigzag-edge spectra $E(k_{e_1})/J$ of the lowest two bands as a function of k_{e_1}. (a) $V = 0J$; (b) $V = 0.3J$; (c) $V = 0.5J$; (d) $V = 1J$. The red solid lines are the representative Fermi levels. The size of the system is 64×89.

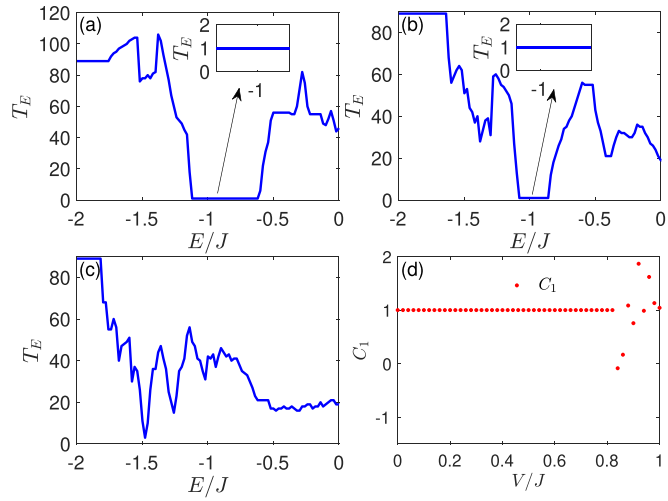

FIG. 4. The transmission coefficient T_E as a function of the Fermi energy with $V = 0.3J$ in (a); $V = 0.6J$ in (b); and $V = J$ in (c). The insets enlarge the stage with $T_E = 1$. (d) The Chern number C_1 versus the potential strength V at 1/3 filling. The size of the system is 40×144.

be obtained from the Landauer formula [45,46],

$$G_E = \frac{2e^2}{h} T_E, \tag{3}$$

where $2e^2/h$ is the unit of G_E and T_E is the transmission coefficient, which is expressed as

$$T_E = \mathrm{Tr}[\Gamma_L G^r \Gamma_R G^a], \tag{4}$$

where G^r (G^a) is the retarded (advanced) Green's function of the system with $G^r = [EI - H_C - \Sigma_L - \Sigma_R]$ and $G^a = (G^r)^\dagger$, and $\Gamma_{L/R} = i[\Sigma_{L/R} - (\Sigma_{L/R})^\dagger]$. We use H_C to denote the Hamiltonian of the system. The self-energies Σ_L and Σ_R are given by

$$\Sigma_L = H_{LC}^\dagger \mathrm{g}_L H_{LC}, \quad \Sigma_R = H_{CR} \mathrm{g}_R H_{CR}^\dagger, \tag{5}$$

where H_{LC} (H_{CR}) denotes the coupling matrices between the system and the L (R) leads, and g_L (g_R) are surface Green's functions of the L (R) leads.

We consider a system size 40×144 with open boundary conditions in $\boldsymbol{e_2}$ and take $V = 0.3J$, $V = 0.6J$, and $V = J$. The transmission coefficients as a function of the Fermi energy are presented in Figs. 4(a), 4(b), and 4(c), respectively. As seen, there is a step with $T_E = 1$ at 1/3 filling in the gapped cases ($V = 0.3J$ and $V = 0.6J$), while in the gapless case ($V = J$), no feature with $T_E = 1$ exists at 1/3 filling. Furthermore, the results of the T_E coincide with the topological phase diagram in Fig. 4(d). In this diagram, $C_1 = 1$ for $V < V_c$, corresponding to $T_E = 1$, while C_1 is unquantized when the potential strength V crosses the critical point V_c, corresponding to the unquantized T_E. The bulk gap is actually closed in this parameter area, which accounts for the appearance of the unquantized Chern number. Hence, there is no topology-protected edge mode, reflecting the trivial nature of the system. On the contrary, the quantized $C_1 = 1$ exactly corresponds to the two edge modes within the bulk gap, presenting the bulk-edge correspondence, and being self-consistent with the two-channel conductance. In addition, the system can be viewed as a one-dimensional tight-binding model in which each unit cell has been replaced with a supercell that contains N_{e_2} cells in the longitudinal direction. The one-dimensional tight-binding model depicts a gapless metal when $V > V_c$. Therefore, in the gapless case, there is no quantized conductance below or above the Fermi energy at 1/3 filling [see Fig. 4(c)], presenting intrinsically metallic transport characteristics of the system.

IV. TRANSVERSE ANDERSON LOCALIZATION TRANSITION

The two-channel transport observation shows that there is no any edge mode and no localization phenomenon along the longitudinal direction when $V > V_c$. We conclude that the Anderson localization in the transverse direction (named as the transverse Anderson localization) is associated with the lack of the edge mode. After all, the localization will prevent the particles from moving toward the boundaries of the system, preventing the system from forming edge states. Meanwhile, it is still to be solved in this 2D quasidisordered Chern insulator without extra magnetic fields whether the topological phase transition is synchronous with the transverse Anderson localization transition. Recent work on the 2D topological superconductors with external magnetic fields shows that the two transitions are asynchronous [28]. We shall describe the localization characteristics of the system using the partial inverse participation ratio (PIPR) in order to verify this hypothesis. The system satisfies PBCs in two directions and has a finite size with $N_{e_2} = F_s$ in the $\boldsymbol{e_2}$ direction but no boundary in the N_{e_1} direction. N_{e_2} is chosen as the Fibonacci number to minimize the size effect. Then, the PIPR of a normalized wave function ψ reads as

$$\mathrm{PIPR} = \sum_{n=0}^{N_{e_2}-1} |\psi(\mathcal{S}_n)|^4 N_{e_1}^2, \tag{6}$$

where the index m has been suppressed (the same below).

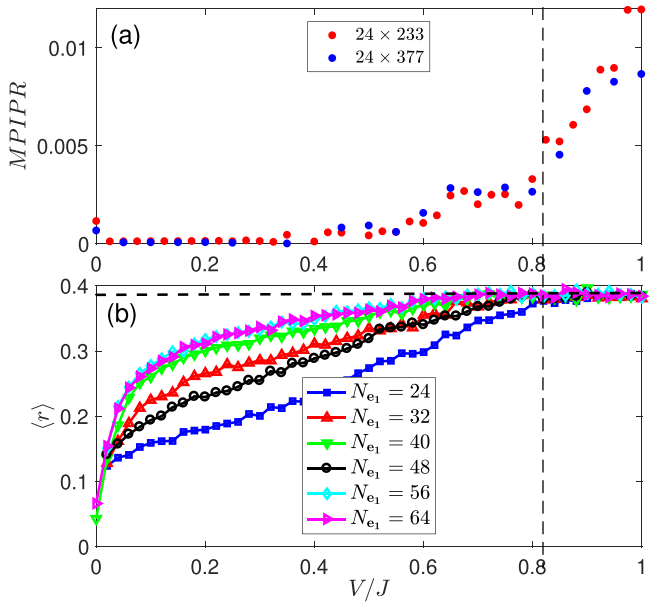

FIG. 5. (a) The MPIPR as a function of the quasiperiodic potential strength V with the system size 24×233 (red dots) and 24×377 (blue dots). The averaged level spacing ratio $\langle r \rangle$ as a function of V is presented in (b) with $N_{\mathbf{e_2}} = 144$, where the horizontal black dashed line corresponds to the Poisson distribution value $\langle r \rangle \approx 0.3863$. The black dashed reference line denotes the critical point.

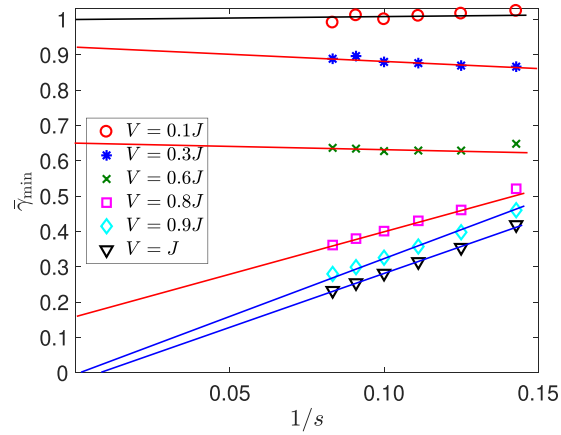

FIG. 6. Plots of $\bar{\gamma}_{\min}$ versus $1/s$ for the wave functions within 1/3 filling.

The wave packets are periodically distributed in the longitudinal direction because there is preserved translational invariance in this direction. In light of the fact that the PIPR in Eq. (6) is a quantity specified in the transverse direction, it is more practical and useful to characterize the localization property in this direction using the PIPR. When the PIPR tends to a finite value, the wave function is localized in the $\boldsymbol{e_2}$ direction. The PIPR scales as F_s^{-1} for the extended states, while it behaves like $F_s^{-\gamma}$ $(0 < \gamma < 1)$ for the critical states. We refer to the extended and the critical states as the delocalized states in the following because they differ significantly from the localized states and the extended (or critical) states. In Fig. 5(a), the corresponding mean PIPR (MPIPR) of the wave functions within the 1/3 filling are presented using two system sizes as examples: 24×233 and 24×377. The black dashed line indicates the key point where the MPIPR intuitively jumps, indicating a transverse Anderson localization transition.

Next, we aim to study the transverse Anderson localization transition by analyzing the energy gap statistic. To perform the analysis, we calculate the average of the energy level spacing ratio $\langle r \rangle$ over the energies within the 1/3 filling, which is defined by $\langle r \rangle = \frac{1}{N_{\mathbf{e_1}} \times N_{\mathbf{e_2}} - 2} \sum_j r_j$, where $r_j = \min\{\delta_j, \delta_{j+1}\}/\max\{\delta_j, \delta_{j+1}\}$ and $\delta_j = E_{j+1} - E_j$ with the energies E_j arranged in an ascending order. In the numerically calculations, we take PBCs and $N_{\mathbf{e_2}} = 144$. Figure 5(b) presents $\langle r \rangle$ as a function of V for various $N_{\mathbf{e_1}}$ at 1/3 filling. More importantly, $\langle r \rangle$ approaches the Poisson distribution value [47,48] $\langle r \rangle_{\text{Poisson}} = 2\ln(2) - 1 \approx 0.3863$ [the horizontal black dashed line in Fig. 5(b)] when the quasidisorder strength V is larger than the critical point. Besides, it is readily seen that $\langle r \rangle$ for various $N_{\mathbf{e_1}}$ are less than 0.3863 when V is smaller than the critical value, presenting the level statistics feature of the single-particle delocalized states [49].

We examine the scaling behavior of the wave functions to further clarify the transverse Anderson localization transition. As previously stated, the wave packets are periodically distributed at each site $\mathcal{S}_n$. The probability $P(\mathcal{S}_n)$ for the sites in the transverse direction is defined as $P(\mathcal{S}_n) = |\psi(\mathcal{S}_n)|^2 N_{\boldsymbol{e_1}}$. Then a scaling index γ_j is given by $P(\mathcal{S}_n) = F_s^{-\gamma_j}$. For a concrete wave function, γ_j will distribute within an interval $[\gamma_{\min}, \gamma_{\max}]$. In the thermodynamic limit $1/s \to 0$, $\gamma_{\min} \to 0$ corresponds to the localized states, while $0 < \gamma_{\min} \leqslant 1$ for the delocalized states (particularly, $\gamma_{\min} = 1$ denotes the extended states; otherwise, it corresponds to the critical states). Therefore, we will employ $\gamma_{\min}$ to characterize the scaling behaviors of the wave functions. In the numerical calculations, we choose $N_{\boldsymbol{e_1}} = 40$ and take PBCs and then average the $\gamma_{\min}$ over the wave functions whose corresponding energies are within the 1/3 filling. We label the averaged $\gamma_{\min}$ by $\bar{\gamma}_{\min} = \frac{1}{N_{\mathbf{e_1}} \times N_{\mathbf{e_2}}} \sum_{j=1}^{N_{\mathbf{e_1}} \times N_{\mathbf{e_2}}} \gamma_{\min}^j$. The extracted $\bar{\gamma}_{\min}$ from the wave functions for different V are plotted in Fig. 6. It is seen that the $\bar{\gamma}_{\min}$ in the extrapolating limit decreases as the quasiperiodic potential strength V increases, and it finally tends to zero when V crosses the critical point V_c, presenting the transverse delocalization-localization phase transition. The results reflected from the $\bar{\gamma}_{\min}$ confirm the prediction of the MPIPR and the energy gap statistics. Therefore, we believe that in this quasidisordered 2D Chern insulator, the topological phase transition is actually synchronous with the transverse Anderson localization transition.

In the previous work, Roati *et al.* prepared a noninteracting Bose-Einstein condensate in a one-dimensional quasiperiodic optical lattice, and observed the exponential Anderson localization [50]; i.e., the wave packet presents the form $|\psi(x)| \propto \exp(-|x - x_0|/\xi)$ with ξ the localization length. Taking a system size with $N_{\boldsymbol{e_1}} \times N_{\boldsymbol{e_2}} = 64 \times 610$ and $V = 0.9J$ in the localized phase, we choose the corresponding ground state as an example to check whether the wave functions in the local-

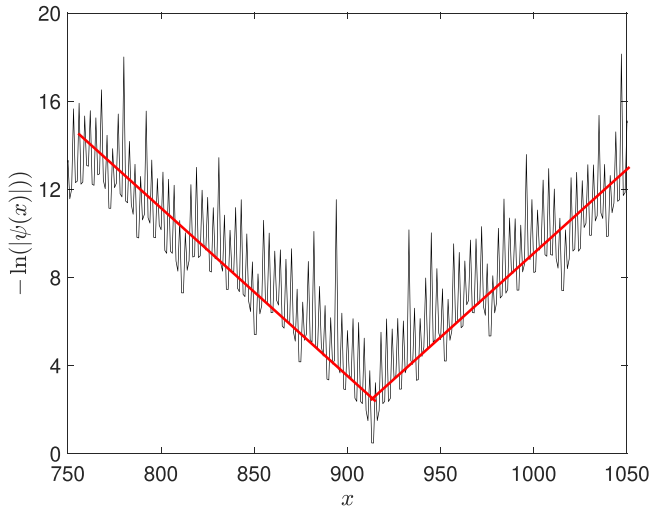

FIG. 7. Exponential localization in the transverse direction. The system size is $N_{e_1} \times N_{e_2} = 64 \times 610$ and $V = 0.9J$. The red lines denote the reference lines.

ized phase are exponentially localized. The negative logarithm of the probability amplitude $|\psi(x)|$ is plotted in the transverse direction as a function of the site x in Fig. 7. Intuitively, the curve presents the linear change on both sides of the minimum, signaling the exponential localization. As a result, we believe that the transverse (exponential) Anderson localization in this 2D quasidisordered system has the potential to be observed in the ultracold atomic experiment.

V. SUMMARY

We have investigated the influence of the quasidisorder on the topological properties and the localization behaviors of a 2D system. The topological phase transition is characterized by the band gap, edge-state spectra, and transport conductance. When a topological transition occurs, the bands gap closes and there are no longer any edge modes. In the gapless phase, the system behaves more like a metal, according to the transport conductance. The results are agreement with the topological diagram which contains the Chern number of the lowest band. In addition, a transverse localization transition is characterized by the MPIPR, level statistics, and the fraction dimension. The findings extend the insight into the synchronicity between the topological phase transition and the transverse Anderson localization, and the reveal the topological nature of the bulk delocalized states.

Note added. Recently, we became aware of the transverse Anderson localization studied in the quasidisordered 2D topological superconductors with magnetic fields (Ref. [28], which is now published in Ref. [28]). The transverse Anderson localization may have potential applications in future cold atom experiments. It implies that in addition to the conventional 1D standing wave method, we can use the transverse Anderson localization to prepare a 1D localized system, and as a result, the 1D cold atom experiments are feasible to be simulated in a 2D system.

ACKNOWLEDGMENTS

We acknowledge support from NSFC under Grants No. 11835011 and No. 12174346.

[1] F. D. M. Haldane, Model for a Quantum Hall Effect without Landau Levels: Condensed-Matter Realization of the "Parity Anomaly", Phys. Rev. Lett. **61**, 2015 (1988).
[2] C.-K. Chiu, J. C. Y. Teo, A. P. Schnyder, and S. Ryu, Classification of topological quantum matter with symmetries, Rev. Mod. Phys. **88**, 035005 (2016).
[3] G. Jotzu, M. Messer, R. Desbuquois, M. Lebrat, T. Uehlinger, D. Greif, and T. Esslinger, Experimental realization of the topological Haldane model with ultracold fermions, Nature (London) **515**, 237 (2014).
[4] C. L. Kane and E. J. Mele, Quantum Spin Hall Effect in Graphene, Phys. Rev. Lett. **95**, 226801 (2005).
[5] M. Z. Hasan and C. L. Kane, Colloquium: Topological insulators, Rev. Mod. Phys. **82**, 3045 (2010).
[6] X.-L. Qi and S.-C. Zhang, Topological insulators and superconductors, Rev. Mod. Phys. **83**, 1057 (2011).
[7] N. Nagaosa, J. Sinova, S. Onoda, A. H. MacDonald, and N. P. Ong, Anomalous Hall effect, Rev. Mod. Phys. **82**, 1539 (2010).
[8] D. J. Thouless, M. Kohmoto, M. P. Nightingale, and M. den Nijs, Quantized Hall Conductance in a Two-Dimensional Periodic Potential, Phys. Rev. Lett. **49**, 405 (1982).
[9] D. Xiao, M.-C. Chang, and Q. Niu, Berry phase effects on electronic properties, Rev. Mod. Phys. **82**, 1959 (2010).
[10] E. Prodan, T. L. Hughes, and B. A. Bernevig, Entanglement Spectrum of a Disordered Topological Chern Insulator, Phys. Rev. Lett. **105**, 115501 (2010).
[11] E. Prodan, Disordered topological insulators: A non-commutative geometry perspective, J. Phys. A: Math. Theor. **44**, 113001 (2011).
[12] E. Abrahams, P. W. Anderson, D. C. Licciardello, and T. V. Ramakrishnan, Scaling Theory of Localization: Absence of Quantum Diffusion in Two Dimensions, Phys. Rev. Lett. **42**, 673 (1979).
[13] D. Z. Liu and S. Das Sarma, Universal scaling of strong-field localization in an integer quantum Hall liquid, Phys. Rev. B **49**, 2677 (1994).
[14] D. Z. Liu, X. C. Xie, and Q. Niu, Weak Field Phase Diagram for an Integer Quantum Hall Liquid, Phys. Rev. Lett. **76**, 975 (1996).
[15] X. C. Xie, X. R. Wang, and D. Z. Liu, Kosterlitz-Thouless-Type Metal-Insulator Transition of a 2D Electron Gas in a Random Magnetic Field, Phys. Rev. Lett. **80**, 3563 (1998).
[16] A. MacKinnon and B. Kramer, One-Parameter Scaling of Localization Length and Conductance in Disordered Systems, Phys. Rev. Lett. **47**, 1546 (1981).
[17] A. MacKinnon and B. Kramer, The scaling theory of electrons in disordered solids: Additional numerical results, Z. Phys. B **53**, 1 (1983).
[18] M. Onoda and N. Nagaosa, Quantized Anomalous Hall Effect in Two-Dimensional Ferromagnets: Quantum Hall Effect in Metals, Phys. Rev. Lett. **90**, 206601 (2003).

[19] M. Onoda, Y. Avishai, and N. Nagaosa, Localization in a Quantum Spin Hall System, Phys. Rev. Lett. **98**, 076802 (2007).

[20] Z. Xu, L. Sheng, D. Y. Xing, E. Prodan, and D. N. Sheng, Topologically protected extended states in disordered quantum spin-Hall systems without time-reversal symmetry, Phys. Rev. B **85**, 075115 (2012).

[21] M. Gonçalves, P. Ribeiro, and E. V. Castro, The Haldane model under quenched disorder, arXiv:1807.11247.

[22] H. Li, C.-Z. Chen, H. Jiang, and X. C. Xie, Coexistence of Quantum Hall and Quantum Anomalous Hall Phases in Disordered $MnBi_2Te_4$, Phys. Rev. Lett. **127**, 236402 (2021).

[23] B. Hetényi, S. Parlak, and M. Yahyavi, Scaling and renormalization in the modern theory of polarization: Application to disordered systems, Phys. Rev. B **104**, 214207 (2021).

[24] D. D. Vu and S. Das Sarma, Weak quantization of noninteracting topological Anderson insulator, Phys. Rev. B **106**, 134201 (2022).

[25] Y. Yang, Z. Xu, L. Sheng, B. Wang, D. Y. Xing, and D. N. Sheng, Time-Reversal-Symmetry-Broken Quantum Spin Hall Effect, Phys. Rev. Lett. **107**, 066602 (2011).

[26] S. Aubry and G. André, Analyticity breaking and Anderson localization in incommensurate lattices, Ann. Isr. Phys. Soc. **3**, 18 (1980).

[27] Y. Fu, J. H. Wilson, and J. H. Pixley, Flat topological bands and eigenstate criticality in a quasiperiodic insulator, Phys. Rev. B **104**, L041106 (2021).

[28] M. F. Madeira and P. D. Sacramento, Quasidisorder-induced topology, Phys. Rev. B **106**, 224505 (2022).

[29] Y.-P. Wu, L.-Z. Tang, G.-Q. Zhang, and D.-W. Zhang, Quantized topological Anderson-Thouless pump, Phys. Rev. A **106**, L051301 (2022).

[30] D. Mao and T. Senthil, Quasiperiodicity, band topology, and moiré graphene, Phys. Rev. B **103**, 115110 (2021).

[31] D. S. Borgnia, A. Vishwanath, and R.-J. Slager, Rational approximations of quasiperiodicity via projected Green's functions, Phys. Rev. B **106**, 054204 (2022).

[32] Q.-B. Zeng and R. Lü, Topological phases and Anderson localization in off-diagonal mosaic lattices, Phys. Rev. B **104**, 064203 (2021).

[33] S. Liu and Q.-Z. Hou, Probing Chern number of quasicrystals with disorders in optical lattices, Quantum Inf. Process. **20**, 132 (2021).

[34] J. Vidal, R. Mosseri, and B. Douçot, Aharonov-Bohm Cages in Two-Dimensional Structures, Phys. Rev. Lett. **81**, 5888 (1998).

[35] J. Vidal, P. Butaud, B. Douçot, and R. Mosseri, Disorder and interactions in Aharonov-Bohm cages, Phys. Rev. B **64**, 155306 (2001).

[36] T. Andrijauskas, E. Anisimovas, M. Račiūnas, A. Mekys, V. Kudriašov, I. B. Spielman, and G. Juzeliūnas, Three-level Haldane-like model on a dice optical lattice, Phys. Rev. A **92**, 033617 (2015).

[37] S. M. Zhang and L. Jin, Compact localized states and localization dynamics in the dice lattice, Phys. Rev. B **102**, 054301 (2020).

[38] J. Li, R.-L. Chu, J. K. Jain, and S.-Q. Shen, Topological Anderson Insulator, Phys. Rev. Lett. **102**, 136806 (2009).

[39] H. Jiang, L. Wang, Q.-F. Sun, and X. C. Xie, Numerical study of the topological Anderson insulator in HgTe/CdTe quantum wells, Phys. Rev. B **80**, 165316 (2009).

[40] C. W. Groth, M. Wimmer, A. R. Akhmerov, J. Tworzydło, and C. W. J. Beenakker, Theory of the Topological Anderson Insulator, Phys. Rev. Lett. **103**, 196805 (2009).

[41] C. P. Orth, T. Sekera, C. Bruder, and T. L. Schmidt, The topological Anderson insulator phase in the Kane-Mele model, Sci. Rep. **6**, 24007 (2016).

[42] J. Song, H. Liu, H. Jiang, Q.-F. Sun, and X. C. Xie, Dependence of topological Anderson insulator on the type of disorder, Phys. Rev. B **85**, 195125 (2012).

[43] J. H. García, L. Covaci, and T. G. Rappoport, Real-Space Calculation of the Conductivity Tensor for Disordered Topological Matter, Phys. Rev. Lett. **114**, 116602 (2015).

[44] Y.-Y. Zhang, R.-L. Chu, F.-C. Zhang, and S.-Q. Shen, Localization and mobility gap in the topological Anderson insulator, Phys. Rev. B **85**, 035107 (2012).

[45] Y. Imry and R. Landauer, Conductance viewed as transmission, Rev. Mod. Phys. **71**, S306 (1999).

[46] S. Datta, *Electronic Transport in Mesoscopic Systems*, Cambridge Studies in Semiconductor Physics and Microelectronic Engineering (Cambridge University Press, Cambridge, UK, 1995).

[47] V. Oganesyan and D. A. Huse, Localization of interacting fermions at high temperature, Phys. Rev. B **75**, 155111 (2007).

[48] A. Pal and D. A. Huse, Many-body localization phase transition, Phys. Rev. B **82**, 174411 (2010).

[49] S. Schiffer, X.-J. Liu, H. Hu, and J. Wang, Anderson localization transition in a robust $\mathcal{PT}$-symmetric phase of a generalized Aubry-André model, Phys. Rev. A **103**, L011302 (2021).

[50] G. Roati, C. D'Errico, L. Fallani, M. Fattori, C. Fort, M. Zaccanti, G. Modugno, M. Modugno, and M. Inguscio, Anderson localization of a non-interacting Bose-Einstein condensate, Nature (London) **453**, 895 (2008).